We are IntechOpen, the world's leading publisher of Open Access books Built by scientists, for scientists

4,800
Open access books available

122,000
International authors and editors

135M
Downloads

Our authors are among the

154
Countries delivered to

TOP 1%
most cited scientists

12.2%
Contributors from top 500 universities

CLARIVATE ANALYTICS BOOK CITATION INDEX INDEXED

WEB OF SCIENCE™

Selection of our books indexed in the Book Citation Index in Web of Science™ Core Collection (BKCI)

Interested in publishing with us?
Contact book.department@intechopen.com

Numbers displayed above are based on latest data collected.
For more information visit www.intechopen.com

Chapter 5

Thermal Hysteresis Due to the Structural Phase Transitions in Magnetization for Core-Surface Nanoparticles

Rıza Erdem, Songül Özüm and Orhan Yalçın

Additional information is available at the end of the chapter

http://dx.doi.org/10.5772/61043

Abstract

One important issue raised in magnetism studies is the thermal response of various magnetic properties. This topic is known as the magnetic thermal hysteresis (MTH) which is principally associated with magnetic phase transitions. The MTH is of particular interest for both quantum and applied physics researches on magnetization of nanomaterials. Hysteresis of the temperature-induced structural phase transitions in some materials and nanostructures with first-order phase transitions reduces useful magnetocaloric effect to transform cycling between martensite (M) and austenite (A) phases under application. In additional, the size, surface and boundary effects on thermal hysteresis loops have been under consideration for the development of research on nanostructured materials. Experimental data indicate that nanostructured materials offer many interesting prospects for the magnetization data and for understanding of temperature-induced M-A phase transitions. In this chapter, we have presented a review of the the latest theoretical developments in the field of MTH related to the structural phase transitions for the core-surface nanoparticles based on the fundamental formulation of pair approximation in Kikuchi version.

Keywords: Thermal hysteresis, Nanoparticles, Martensite, Austenite, Pair approximation

1. Introduction

The phenomenon of hysteresis is encountered in many areas of physics. It is associated with the delay of the dynamic response of cooperative systems to external perturbation. During a heating–cooling process in a system, thermal hysteresis (TH) commonly appears accompanying phase transitions. In particular, it is regarded as a signature of the first-order phase transition. But, the TH is less known than the magnetic hysteresis (MH), which is another type

of hysteresis in magnetism [1]. Rao and Pandit [2] studied both TH and MH, and they found that TH seems to belong to a different universality class than MH in the same relaxational model.

One important issue raised in magnetism studies is the thermal response of various magnetic properties. This topic is known as the magnetic thermal hysteresis (MTH) or TH in magnetization, which is principally associated with magnetic phase transitions (MPTs). Many bulk materials with MPTs have been discovered to exhibit significant MTH behaviour. Among those materials, well known samples are spin crossover compounds [3–8], manganites [9], superconductors [10, 11], magnetic multilayers [12, 13], ferrimagnetic and metamagnetic alloys [14, 15], polycrystalline samples [16], manganite thin films [17] and manganite perovskites [18]. Thermal hysteresis occurs in these samples because the transitions between various magnetic phases occur at different temperatures for the heating and cooling processes. Furthermore, the temperature span of the TH can be substantially reduced by applying an external magnetic field. The thermoelastic austenite–martensite transformations in Heusler and shape memory alloys were also characterized by the TH loops [19–21].

Apart from the above investigations of bulk systems, the MTH is of particular interest for both quantum and applied physics researches on magnetization of nanomaterials. Several groups studied some important physical properties of various types of nanostructures using the properties of TH loops. For example, from the thermal response of conductivity for the gold nanoparticles (NPs), a phase transition phenomenon was revealed by a temperature criticality by Sarkar et al. [22]. Based on Ising-like treatment of the MTH and using Monte Carlo algorithm, Kawamoto and Abe [23] obtained smaller hysteresis width when the volume of the spin crossover NPs was decreased. Also, using the same treatment, the simulated hysteretic loops become closer to the experimental ones [24, 25].

On the other hand, hysteresis of the temperature-induced structural phase transitions in nanostructures with first-order phase transitions reduce useful magnetocaloric effect to transform cycling between martensite (M) and austenite (A) phases under application. In addition, the size, surface and boundary effects on thermal hysteresis loops have been under consideration for the development of research on nanostructured materials. Experimental data indicate that nanostructured materials offer many interesting prospects for the magnetization data and for understanding of temperature-induced martensite/austenite phase transitions.

In this chapter, we shall review the latest theoretical developments in the field of MTH related to the structural phase transitions for the core/surface (*C*/*S*) NPs based on the fundamental formulation of pair approximation in Kikuchi version.

2. Basics of the theoretical model

2.1. Definition of a nanoparticle with core/surface morphology

For a noninteracting spherical nanoparticle, arrays of spins are generally considered on a hexagonal lattice in 2D, as shown in Fig. 1 [26]. This structure may also be extended to hexagonal closed packed (hcp) lattice for any three-dimensional (3D) case which is not covered

http://dx.doi.org/10.5772/61043

in Fig. 1 but is illustrated in a recent publication by Yalçın et al. [27]. Similarly, a square lattice in 2D (shown in Fig. 2) is enlarged to simple cubic lattice (sc) in 3D for a cubic nanoparticle. For the number of shells in both structures, each lattice is related to the radius (R) of the nanoparticle [27–29]. Therefore, the value of R contains a number of shells and the size of a nanoparticle increases as the number of shells increases. The shells (R) and their numbers are only bounded to the nearest-neighbour pair exchange interactions (J) between spins. To provide the magnetization of the whole particle, each of the spin sites, which stand for the atomistic moments in the nanoparticle, are described by Ising spin variables that take on the values $S_i = \pm 1, 0$. For a core/surface (C/S) morphology, all spins in the nanoparticle are organized in three components that are core (C, filled circles), interface (or core-surface) (CS) and surface (S, empty circles) parts. The number of spins in these parts within the C/S-type nanoparticle are denoted by N_C, N_{CS} and N_S, respectively. But, the total number of spins (N) in a C/S nanoparticle covers only C and S spin numbers, i.e. $N = N_C + N_S$. On the other hand, the numbers of spin pairs for C, CS and S regions in 2D are defined by $N_P^C = (N_C\gamma_C/2) - N_{CS}$, $N_P^{CS} = 2N_{CS}\gamma_{CS}/2$ and $N_P^S = N_S\gamma_S/2$, respectively, where the lattice coordination numbers of the regions are $\gamma_C = 6$, $\gamma_{CS} = \gamma_S = 2$ for hexagonal lattice and $\gamma_C = 4$, $\gamma_{CS} = 2$, $\gamma_S = 0$ for square lattice.

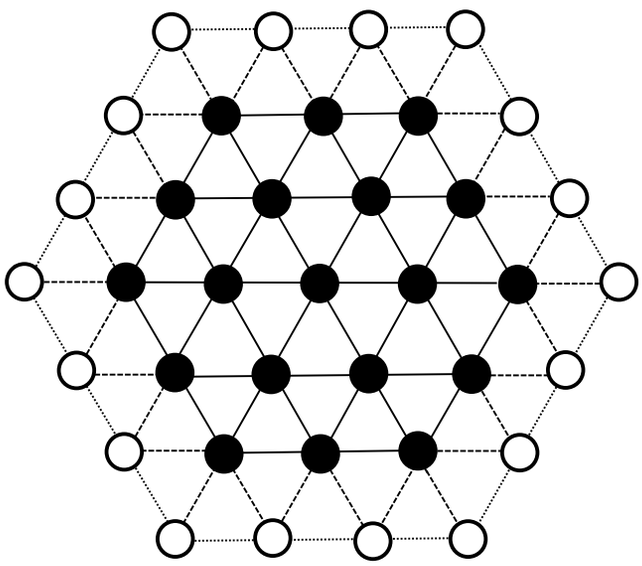

Figure 1. Schematic representation of a nanoparticle on a hexagonal lattice in 2D exhibiting three shells of spins. Filled and empty circles represent the core and surface atoms while solid, dashed and dotted lines correspond to core, core/surface and surface pairs, respectively.

2.2. Blume–Emery–Griffiths model

The Blume–Emery–Griffiths (BEG) model is one of the well-known spin lattice models in equilibrium statistical mechanics. It was originally introduced with the aim to account for phase separation in helium mixtures [30]. Besides various thermodynamic properties, the model has been extended to study the structural phase transitions in many bulk systems. By

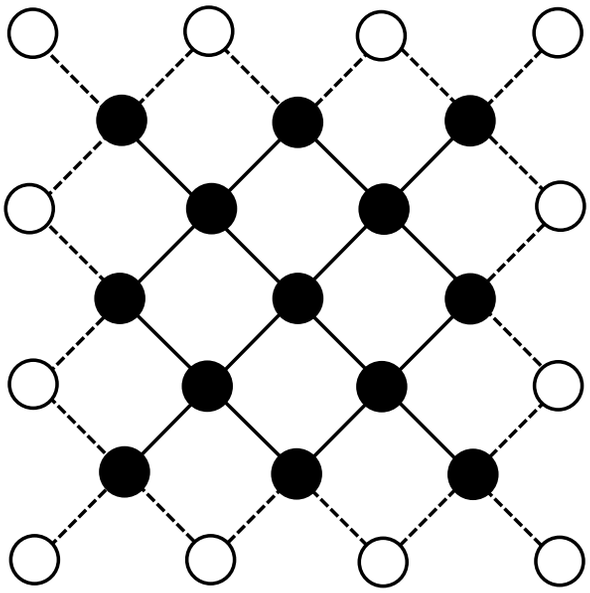

Figure 2. Same as Fig. 1 but for a nanoparticle on a square lattice.

means of mean-field theory (MFT) and Monte Carlo (MC) simulations, magnetostructural phase transitions in some alloys were described via degenerate BEG models in terms of magnetoelastic interactions [31]. In the light of above applications, we have recently used the ordinary BEG model for the investigation of MT/AT transitions in NP systems and observed the behaviours of the MTH loops [28, 29]. In the following, we mention briefly the definition of the BEG Hamiltonian and show clearly how it is modified for the *C*/*S* NPs with hexagonal and square lattice structures.

For a spin configuration $\{S_i\}$, the ordinary BEG model is described by the Hamiltonian

$$H\{S_i\} = -J\sum_{\langle i,j\rangle} S_i S_j - K\sum_{\langle i,j\rangle} S_i^2 S_j^2 - D\sum_{\langle i,j\rangle}(S_i^2 + S_j^2) - h\sum_{\langle i,j\rangle}(S_i + S_j), \tag{1}$$

where $<i, j>$ indicates a sum over the nearest neighbours. J, K, D, h denote, respectively, the dipolar (or bilinear) exchange energy between nearest-neighbour spins, the quadrupolar (or biquadratic) exchange coupling, the single-ion anisotropy constant (or crystal-field parameter) and the external magnetic field. The above parameters are in units of kT (k Boltzmann constant and T temperature). Using various techniques, the model has been analyzed globally, for both negative (J, $K < 0$) and positive (J, $K > 0$) interactions, to obtain the equilibrium phase properties [32, 33]. Here, $J < 0$ and $J > 0$ cases correspond to ferromagnetic (FM) and antiferromagnetic (AFM) dipolar interactions, respectively. When $J = 0$, a paramagnetic (PM) character exists in the system for all temperatures. Similarly, the cases $K < 0$ and $K > 0$ describe the repulsive and attractive biquadratic interactions, respectively, and determine the rich phase diagrams with multicritical topology [33]. In the case of $K = 0$, the model is known as the Blume–Capel (BC) model.

http://dx.doi.org/10.5772/61043

The model Hamiltonian (Eq. 1) is now divided into three parts for the *C*/*S* NPs given by $H = H_C + H_{CS} + H_S$ with

$$\begin{aligned} H_C &= -J_C \sum_{\langle i,j \rangle} S_i S_j - K_C \sum_{\langle i,j \rangle} S_i^2 S_j^2 - D_C \sum_{\langle i,j \rangle} (S_i^2 + S_j^2) - h \sum_{\langle i,j \rangle} (S_i + S_j), \\ H_{CS} &= -J_{CS} \sum_{\langle i,j \rangle} S_i \sigma_j - K_{CS} \sum_{\langle i,j \rangle} S_i^2 \sigma_j^2, \\ H_S &= -J_S \sum_{\langle i,j \rangle} \sigma_i \sigma_j - K_S \sum_{\langle i,j \rangle} \sigma_i^2 \sigma_j^2 - D_S \sum_{\langle i,j \rangle} (\sigma_i^2 + \sigma_j^2) - h \sum_{\langle i,j \rangle} (\sigma_i + \sigma_j), \end{aligned} \tag{2}$$

where S_i and σ_i are named as the *C* and *S* spin variables, respectively. In Eq. (2) J_C, J_{CS}, J_S are the bilinear and K_C, K_{CS}, K_S are the biquadratic exchange interactions for *C, CS* and *S* spins, respectively. Moreover, single-ion anisotropy parameters for *C* and *S* spins are denoted by the letters D_C and D_S, respectively. If $J_C = J_{CS} = J_S = J_0$ and $K_C = K_{CS} = K_S = K_0$ the particle is known as homogeneous (HM) nanoparticle while one of the conditions $J_C \neq J_{CS} \neq J_S$, $J_C = J_{CS} \neq J_S$, $J_C \neq J_{CS} = J_S$, $J_{CS} \neq J_C = J_S$, $K_C \neq K_{CS} \neq K_S$, $K_C = K_{CS} \neq K_S$, $K_C \neq K_{CS} = K_S$, $K_{CS} \neq K_C = K_S$ corresponds to a composite (CM) nanoparticle.

2.3. Fundamental formulation of pair approximation in Kikuchi version

In the pair approximation proposed by Kikuchi [34], each spin case is indicated by p_i, which is also so entitled the point or state variables. These point/state variables obey the normalization relation

$$\sum_i p_i = 1. \tag{3}$$

Using the pair correlations between spins, another types of internal (or bond/pair) variables denoted by P_{ij} are introduced. P_{ij} (with a symmetry $P_{ij} = P_{ji}$) means the medial number of the states in which the first members of the nearest-neighbour pair is in state *i* and second member in state *j*. The bond variables are also normalized by

$$\sum_{i,j} P_{ij} = 1, \tag{4}$$

and connected with state variables through the relations

$$p_i = \sum_{i,j} P_{ij}. \tag{5}$$

In order to determine an expression for the bond variables, we define the interaction energy (E) and entropy (S_E) of system in terms of these variables as

$$\beta E = N\frac{\gamma}{2}\sum_{i,j}\varepsilon_{ij}P_{ij}, \tag{6}$$

$$S_E = Nk\left((\gamma-1)\sum_{i,j}p_i\ln(p_i) - \frac{\gamma}{2}\sum_{i,j}P_{ij}\ln(P_{ij})\right), \tag{7}$$

where $\beta=1/kT$, γ is the coordination number for a lattice site and N is the number of these sites. The ε_{ij} parameters in Eq. (6) are called the bond energies for the spin pairs (i, j) and determined from Eq. (1). The free energy (Φ) per site can be found from

$$\Phi = \frac{\beta F}{N} = \frac{\beta}{N}(E - TS_E). \tag{8}$$

The minimization of Eq. (8) with respect to P_{ij} ($\partial\Phi/\partial P_{ij}=0$) leads to the following set of self-consistent equations for the system at equilibrium:

$$P_{ij} = Z^{-1}(p_i p_j)^{(\gamma-1)/\gamma}\exp(-\beta\varepsilon_{ij}) \equiv Z^{-1}e_{ij}, \tag{9}$$

where Z is the partition function:

$$Z = \exp(2\beta\lambda/\gamma) = \sum_{i,j}e_{ij}. \tag{10}$$

Here, λ is introduced to maintain the normalization condition. In many works in the literature, Eq. (9) was easily applied to investigate magnetic properties of various spin models for the bulk materials [35, 36]. But, for the applications to the magnetic NPs systems, one needs to define the energy parameters ε_{ij} appearing in Eq. (9) as

$$\varepsilon_{ij} = N_P^C\varepsilon_{ij}^C + N_P^{CS}\varepsilon_{ij}^{CS} + N_P^S\varepsilon_{ij}^S, \tag{11}$$

where bond energies ε_{ij}^C, ε_{ij}^{CS} and ε_{ij}^S of three regions are found using Eq. (2) as listed in Table 1. The average magnetization (M) of the nanoparticle is the excess of one orientation over the other orientation, also named the dipole moment. It is found from the definition

http://dx.doi.org/10.5772/61043

$$M = P_{++} + P_{+0} + P_{+-} - (P_{-+} + P_{-0} + P_{--}) \tag{12}$$

Using the numerical solutions of Eq. (9) by the iteration technique, the MTH curves are drawn easily from Eq. (12). For some selected exchange energies, the MTH behaviours and the temperature-induced M–A phase transitions within the *C*/*S* smart NPs are reproduced from our recent publications [28, 29] as in Figs. 3–6.

	C	**CS**	**S**
ε_{++}	$-J_C - K_C - 2D_C - 2h$	$-J_{CS} - K_{CS}$	$-J_S - K_S - 2D_S - 2h$
ε_{+0}	$-D_C - h$	0	$-D_S - h$
ε_{+-}	$+J_C - K_C - 2D_C$	$+J_{CS} - K_{CS}$	$+J_S - K_S - 2D_S$
ε_{0+}	$-D_C - h$	0	$-D_S - h$
ε_{00}	0	0	0
ε_{0-}	$-D_C + h$	0	$-D_S + h$
ε_{-+}	$+J_C - K_C - 2D_C$	$+J_{CS} - K_{CS}$	$+J_S - K_S - 2D_S$
ε_{-0}	$-D_C + h$	0	$-D_S + h$
ε_{--}	$-J_C - K_C - 2D_C + 2h$	$-J_{CS} - K_{CS}$	$-J_S - K_S - 2D_S + 2h$

Table 1. Bond energies for the *C*/*S* nanoparticle

3. Calculations and discussion

3.1. Thermal hysteresis for hexagonal nanoparticles

We firstly analyze the MTH loops for the homogeneous hexagonal nanoparticles (HM-HNPs) using $J_C = J_{CS} = J_S = J_0 = 1.0$; $K_C = K_{CS} = K_S = K_0 = -0.6$ under zero magnetic field ($h = 0.0$). Fig. 3 represents the behaviours of these loops for the particles with $R = 4$ and $R = 5$ shells. In the figure, each coloured curve is drawn for one value of single-ion anisotropy (D_0) with $D_C = D_S = D_0$. The thermal behaviour of the particles' magnetization is somewhat different from that of bulk materials. We see clearly (Figs. 3a and 3b) that the magnetization returns to the original point after a complete cycle. The cycles are a specific class of both major and minor hysteretic loops, for which the temperature is reversed only once. For a structural transition, the heating/cooling modes are to be distinguished. Each coloured curve represents both heating and cooling processes according to directions of the arrows. Therefore, the calculations start at a low temperature below the austenite start temperature (A_S) where the magnetization starts to increase sharply until the austenite finish temperature (A_F) is reached. The structure between these two temperatures with $A_S < A_F$ corresponds to a strongly austenite phase. After passing through a maximum, the magnetization decreases as the temperature increases and converges

to zero from another austenite finish temperature A_{F1} to austenite start temperature A_{S1} where we observe a weakly austenite phase with $A_{F1} < A_{S1}$. On the other hand, the cooling process concerns the structural changes associated with martensitic transitions. This may cause an abrupt change of magnetization where a weak martensite phase occurs. The new characteristic temperatures related to the increase in magnetization are denoted by M_{S1} and M_{F1} ($M_{S1} < M_{F1}$) corresponding to martensitic start and martensitic finish temperatures, respectively. As is illustrated at the right columns of each figure in Fig. 3, each coloured curve for the heating/cooling processes coincides with each other at M_{S1} and A_{F1} while they do not coincide at the temperatures M_{F1} and A_{S1}. Further decreasing of the temperature leads to a strongly martensite state, which starts at M_S and ends at M_F. Thus, we have two separate MTH loops; one is at the lower temperature (or the major thermal hysteresis) while the other occurs at larger temperatures (minor thermal loops). For the major case, we note that the loops shift to the higher temperatures and the actual loop area becomes smaller after the decrease of D_0. But, the minor loop shifts to the lower temperatures while the amount of the hysteresis remains approximately the same. A direct comparison of the left/right panels of Fig. 3a with those of Fig. 3b shows how the particle size correlates with all characteristic temperatures.

For understanding the features associated with the MTH behaviours in composite hexagonal nanoparticles (CM-HNPs), we have proceeded to calculate the magnetization as a function of temperature for the same system, but using $J_{CS} = -J_0$ instead of $J_{CS} = J_0$, whose results are shown in Figs. 4a and 4b. Again, we consider four- and five-shell NPs under zero magnetic field (h = 0.0). The new values of D_0 associated with the observation of MT/AT structural phase transitions are listed in each figure. In this case, the small positive values of the single-ion anisotropy are needed for the generic property of MTH loops presented in the previous figure. As demonstrated by Fig. 4, the AFM *C*/*S* dipolar interaction with $J_{CS} = -J_0$ also influences the heights, widths and the positions of the major and minor loops presented in Fig. 3. This fact states that, at constant R and K_0, all characteristic temperatures are decreasing functions of D_0 which determine the smoothness of the reversal. The small hysteresis loops seen in Fig. 4a indicate that the friction to resist the structural transformation is small. According to Hu et al. [15], the small thermal hysteresis is the aspiration of an engineer in applying the materials in magnetocaloric refrigeration. This makes the present CM-HNPs attractive for real applications in new technologies [37].

3.2. Thermal hysteresis for cubic nanoparticles

Another class of small particles known in the literature are called cubic nanoparticles (CNPs). The CNPs attach face-to-face to the surrounding particles. They can form a 2D square array instead of hexagonal ones (Fig. 2). The square array is one of the closed-packed arrangements and the CNPs with a square array have large surface to volume ratios. Owing to their different electronic properties, in recent years, the CNPs received much attention for applications mostly in material science, sensor technology and semiconductor devices. But, the magnetic properties have been very sensitive to the particle shape due to dominating role of surface anisotropy in its magnetization. Compared to the spherical nanoparticles (SNPs), the flat surface of CNPs enabled the surface metal captions to possess a more symmetric coordination. So, the surface

http://dx.doi.org/10.5772/61043

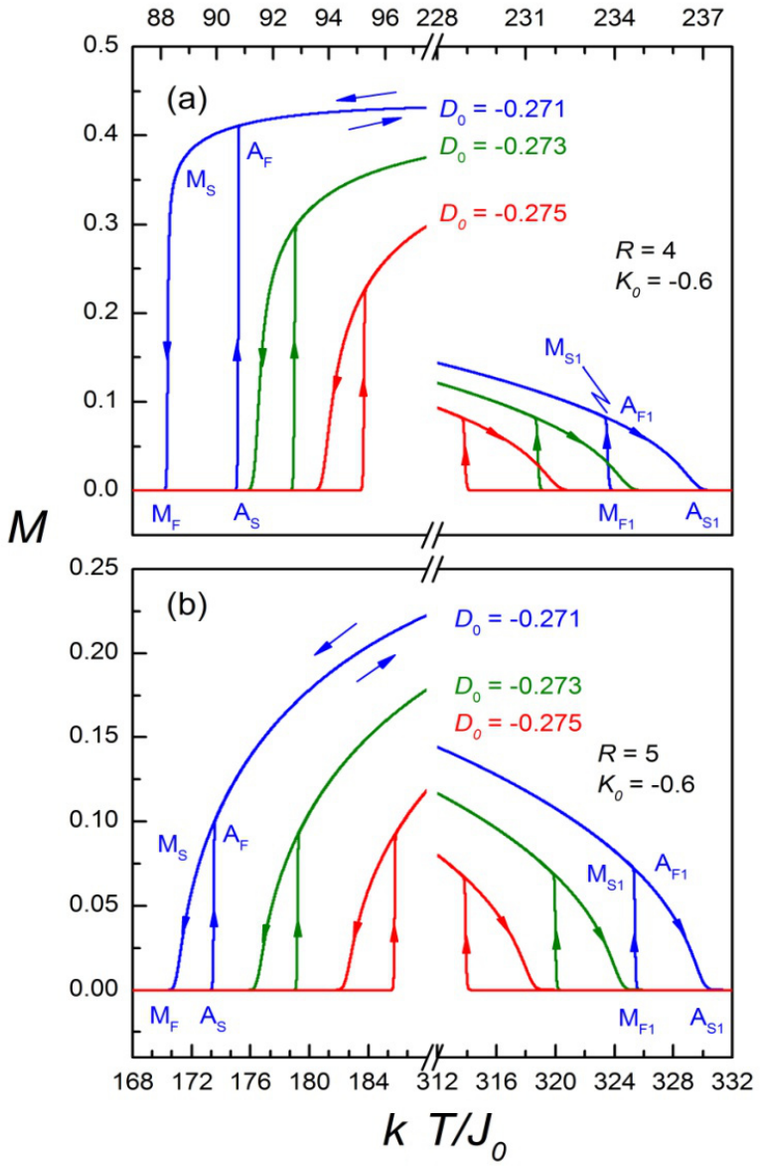

Figure 3. Magnetic thermal hysteresis loops for the HM-HNPs with (a) $R = 4$ and (b) $R = 5$ shells. $J_C = J_{CS} = J_S = J_0 = 1.0$; $K_C = K_{CS} = K_S = K_0 = -0.6$; $D_C = D_S = D_0$ and $h = 0.0$.

anisotropy in the CNPs should be much smaller than the one in HNPs and SNPs. If the magnetic anisotropy of the CNPs is cubic, all such six directions are magnetically identical, and hence the magnetically ordered assembly is greatly simplified. The anisotropy of the growth rate can be ascribed to a different adhesion of the stabilizer on the growing surface. The stabilizer species is the only parameter which was changed to obtain cubical shapes instead of spheres. Because of the above properties, the single-domain CNPs with surface anisotropy were widely investigated using various numerical methods [38–42].

For the sake of comparison with that of HNPs, we here reestablish the MTH curves of the homogeneous cubic nanoparticles (HM-CNPs) and composite cubic nanoparticles (CM-CNPs) by using the same procedure as in the preceding section (Figs. 3 and 4) and focus on the

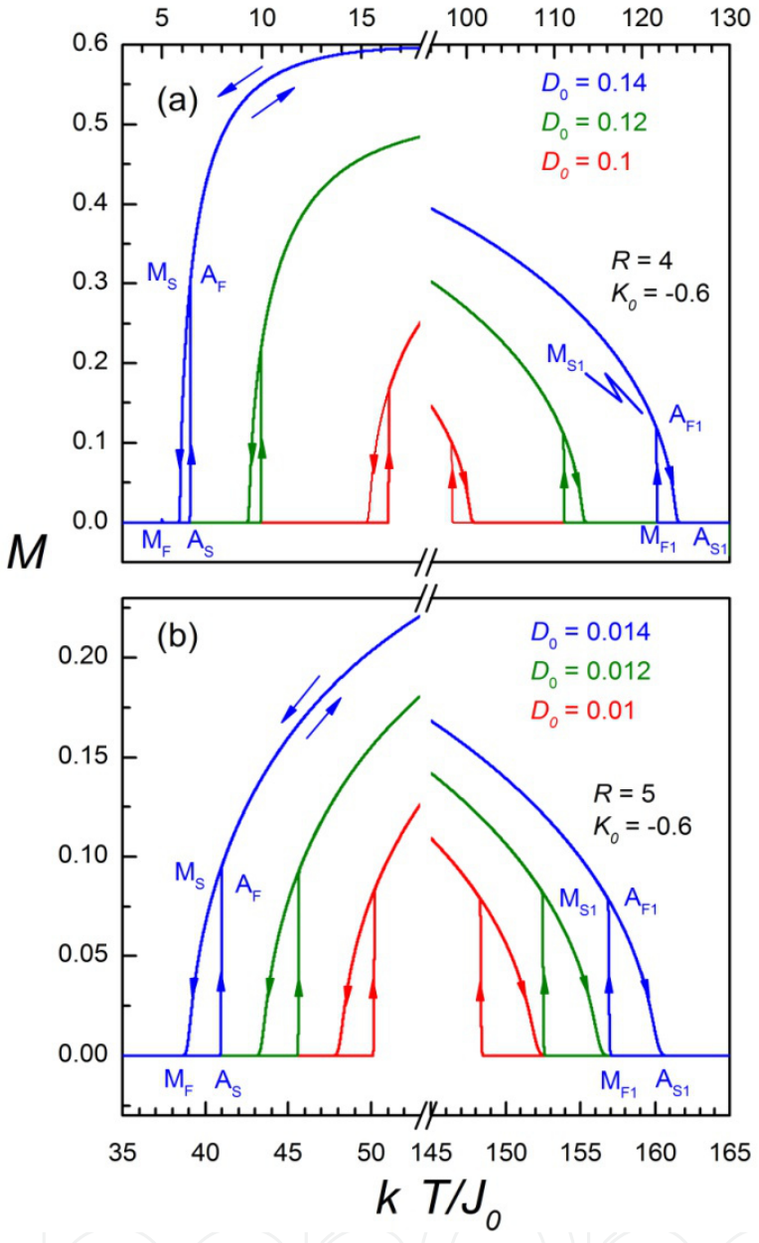

Figure 4. Same as Fig. 3 but for the CM-HNPs with $J_{CS} = -J_0$.

important difference between the martensitic and austenitic transition temperatures, derived from these hysteresis loops, for the CNPs and HNPs. The general aspects of the MTH loops for the CNPs displayed in Figs. 5 and 6 are similar to one for the HNPs given in Figs. 3 and 4. But, the loops are calculated using bigger particles ($R = 6$ and $R = 7$ shells) with greater single-ion anisotropy values, which determine the smoothness of the reversal. It is observed that the transition temperatures diminish when reducing the nanoparticles size in correlation with a smoother conversion, seen in Figs. 5a and 5b. In addition, while the NP sizes are increasing, the single-ion anisotropy parameter also increases and thermal hysteresis loop appears as a rectangular-shaped loop ($D_0 = -0.265$) as shown in Fig. 5b. The single-ion anisotropy parameter

http://dx.doi.org/10.5772/61043

decreases at the larger radius values for the CM-CNPs in Figs. 6a and 6b. If we compare the HM-NPs and CM-NPs, it can be seen that magnetization shows almost the same values but, the transition temperatures of MTH loops for HM-NPs occurred at higher values.

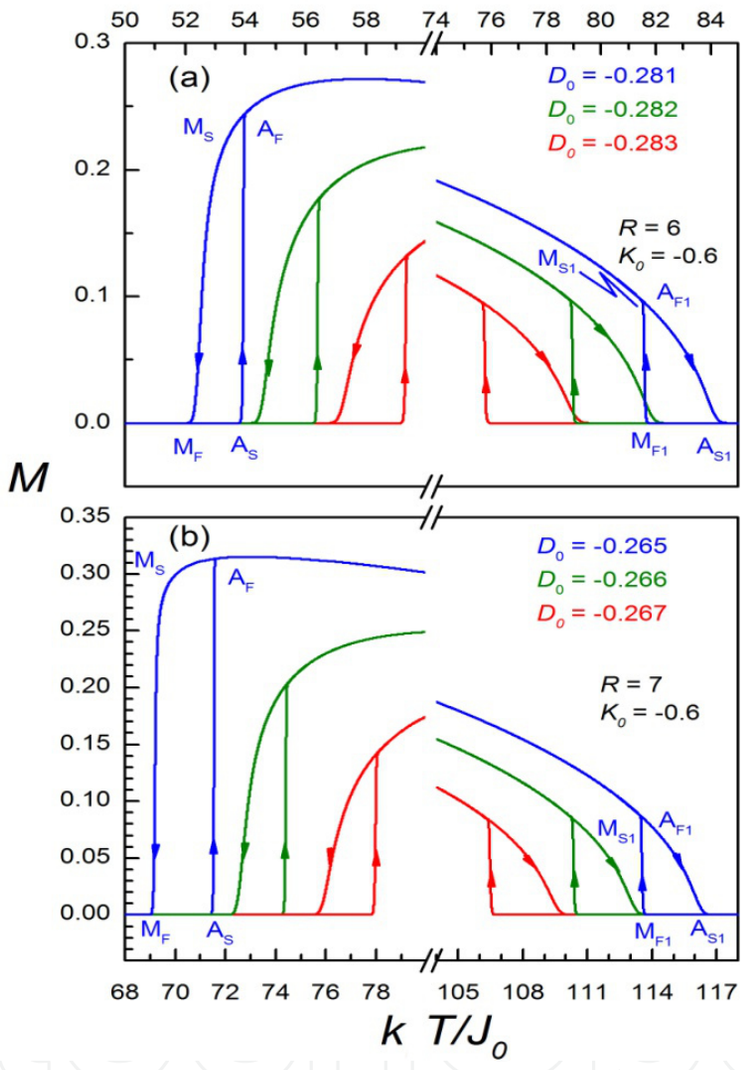

Figure 5. Same as Fig. 3 but for a HM-CNPs with (a) $R = 6$ and (b) $R = 7$ shells.

In general, the thermal hysteresis becomes weaker but, nevertheless, does not disappear completely with increasing NP sizes for the CM-NPs. All loops widen as R decreases for both HM-HNPs and HM-CNPs. Also, a large decrease in transition temperatures occur when the particle structure changes from hexagonal to cubic array. The CNPs ensure that all magnetic properties are well understood because of their easily recognizable magnetization axes and well-defined crystallographic surfaces.

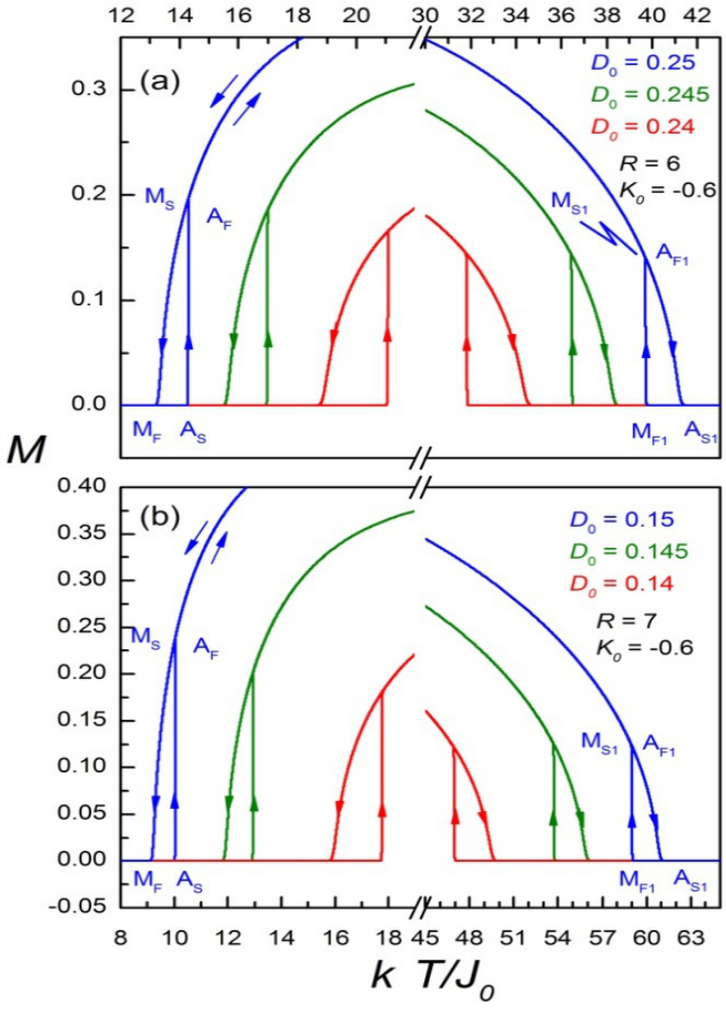

Figure 6. Same as Fig. 4 but for a CM-CNPs with (a) $R = 6$ and (b) $R = 7$ shells.

4. Conclusion

In this chapter, we have presented a review of thermal reversal properties of the *C*/*S* NPs related with the martensitic/austenitic phase transitions. These properties have been recently studied using a powerful statistical mechanics approach called the pair approximation technique. According to the theoretical calculations performed for the hexagonal and cubic NPs at a given particle radius, magnetization versus temperature variations are essentially two closed loops, i.e. MTH curves or loops because of the structural phase transitions from M state to A state (or from A phase to M phase) during heating–cooling processes.

Our review draws a number of important physical properties for the MTH curves regarding the sign of the quadrupolar interactions (K_0) and the values of sing-ion anisotropy (D_0) within the NPs. (1) During heating–cooling processes, we observe TH behaviours for the particles' magnetization, which is indicative of a first-order transition when the quadrupolar interaction is repulsive. The positions and shapes of the loops and the loop area depend on the values of crystal-field parameter as well as the size of the particle. (2) We also show that the thermal

evolution of the magnetization separates the TH loops into two different regions, which have different ordering temperatures. In other words, we observe two TH loops; one (major loop) is at lower temperatures and the other (minor loop) at higher temperatures. (3) We fully explain the thermal reversal process and show that the temperatures at which the NPs reverses its magnetization depend on the applied external magnetic fields while the single-ion anisotropy determines the width and smoothness of the reversal. (4) Most important is the fact that, by varying *C*/*S* dipolar interaction from FM-type to AFM-type as well as by changing crystal field parameter from negative to positive values, a very small TH loop can be obtained and the structural transition temperatures can be turned over a small range of working temperatures.

Acknowledgements

One of the authors (RE) acknowledges the financial support from the Scientific Research Projects Coordination Unit of Akdeniz University.

Author details

Rıza Erdem[1*], Songül Özüm[2] and Orhan Yalçın[3]

*Address all correspondence to: rerdem@akdeniz.edu.tr

1 Department of Physics, Akdeniz University, Antalya, Turkey

2 Institute of Sciences, Niğde University, Niğde, Turkey

3 Department of Physics, Niğde University, Niğde, Turkey

References

[1] Mamiya H, Jeyadevan B. Magnetic hysteresis loop in a superparamagnetic state. IEEE Transactions on Magnetics. 2014; 50: 4001604. DOI: 10.1109/TMAG.2013.2274072.

[2] Rao M, Pandit R. Magnetic and thermal hysteresis in the *O(N)*-symmetric $(\Phi)^2$ model. Physical Review B. 1991; 43; 3373–3386. DOI: 10.1103/PhysRevB.43.3373.

[3] Enachescu C, Machado HC, Menendez N, Codjovi E, Linares J, Varret F, Stancu A. Static and light induced hysteresis in spin-crossover compounds: experimental data and application of Preisach-type models. Physica B. 2001; 306: 155–160. DOI: 10.1016/S0921-4526(01)00996-6.

[4] Linares J, Enachescu C, Boukheddaden K, Varret F. Monte Carlo entropic sampling applied to spin crossover solids: the squareness of the thermal hysteresis loop. Polyhedron. 2003; 22: 2453–2456. DOI: 10.1016/S0277-5387(03)00219-5.

[5] Tanasa R, Enachescu C, Stancu A, Linares J, Codjovi E, Varret F, Haasnoot J. First-order reversal curve analysis of spin-transition thermal hysteresis in terms of physical-parameter distributions and their correlations. Physical Review B. 2005; 71: 014431(1)-014431(9). DOI: 10.1103/PhysRevB.71.014431.

[6] Enachescu C, Tanasa R, Stancu A, Varret F, Linares J, Codjovi E. First-order reversal curves analysis of rate-dependent hysteresis: The example of light-induced thermal hysteresis in a spin-crossover solid. Physical Review B. 2005; 72: 054413(1)–054413(7). DOI: 10.1103/PhysRevB.72.054413.

[7] Stoleriu L, Chakraborty P, Hauser A, Stancu A, Enachescu C. Thermal hysteresis in spin-crossover compounds studied within the mechanoelastic model and its potential application to nanoparticles. Physical Review B. 2011; 84: 134102(1)–134102(9). DOI: 10.1103/PhysRevB.84.134102.

[8] Rotaru A, Graur A, Rotaru G–M, Linares J, Garcia Y. Influence intermolecular interactions and size effect on LITH-FORC diagram in 1D spin-crossover compounds. Journal of Optoelectronics and Advanced Materials. 2012; 14: 529–536.

[9] Dho J, Kim WS, Hur NH. Anomalous thermal hyteresis in magnetization and resistivity of $La_{1-x}Sr_xMnO_3$. Physical Review Letters. 2001; 87: 187201(1)–187201(4). DOI: 10.1103/PhysRevLett.87.187201.

[10] Panagopoulos C, Majoros M, Petrović AP. Thermal hyteresis in the normal-state magnetization of $La_{2-x}Sr_xCuO_4$. Physical Review B. 2004; 69: 144508(1)–144508(7). DOI: 10.1103/PhysRevB.69.144508.

[11] Hissa J, Kallio A. Comment on ''Thermal hyteresis in the normal-state magnetization of $La_{2-x}Sr_xCuO_4$''. Physical Review B. 2005; 72: 176501(1)–176501(3). DOI: 10.1103/PhysRevB.72.176501.

[12] Camley RE, Lohstroh W, Felcher GP, Hosoito N, Hashizume H. Tunable thermal hysteresis in magnetic multilayers: magnetic superheating and supercooling. Journal of Magnetism and Magnetic Materials. 2005; 286: 65–71. DOI: 10.1016/j.jmmm.2004.09.041.

[13] Dantas AL, Camley RE, Carriço AS. Magnetic thermal hysteresis in $Fe_m/Dy_n/Fe_m$ and $Gd_m/Dy_n/Gd_m$ trilayers. Physical Review B. 2007; 75: 094436(1)–094436(6). DOI: 10.1103/PhysRevB.75.094436.

[14] Andrés JP, González JA, Hase TPA, Tanner BK, Riveiro JM. Artificial ferrimagnetic structure and thermal hysteresis in $Gd_{0.47}/Co_{0.53}/Co$ multilayers. Physical Review B. 2008; 77: 144407(1)–144407(7). DOI: 10.1103/PhysRevB.77.144407.

[15] Hu FX, Wang J, Shen J, Gao B, Sun JR, Shen BG. Large magnetic entropy change with small thermal hyteresis near room temperature in metamagnetic alloys $Ni_{51}Co_{49-x}In_x$. Journal of Applied Physics. 2009; 105: 07A940(1)–07A940(3). DOI: 10.1063/1.3073951.

[16] Trung NT, Ou ZQ, Gortenmulder TJ, Tegus O, Buschow KHJ, Brück E. Tunable thermal hysteresis in MnFe(P,Ge) compounds. Journal of Applied Physics. 2009; 94: 102513(1)–102513(3). DOI: 10.1063/1.3095597.

[17] Singh S, Fitzsimmons MR, Lookman T, Thompson JD, Jeen H, Biswas A, Roldan MA, Varela M. Magnetic nonuniformity and thermal hyteresis of magnetism in a manganite thin film. Physical Review Letters. 2012; 108: 077207(1)–077207(5). DOI: 10.1103/PhysRevLett.108.077207.

[18] Wang L, Cui YG, Wan JF, Zhang JH, Rong YH. Magnetic thermal hysteresis due to paramagnetic–antiferromagnetic transition in Fe-24.4Mn-5.9Si-5.1Cr alloy. AIP Advances. 2013; 3: 082126(1)–082126(8). DOI: 10.1063/1.4819483.

[19] Krenke T, Acet M, Wassermann EF, Moya X, Moñosa L, Planes A. Martensitic transitions and the nature of ferromagnetism in the austenitic and martensitic states of Ni-Mn-Sn alloys. Physical Review B. 2005; 72: 014412(1)–014412(9). DOI: 10.1103/PhysRevB.72.014412.

[20] Shamberger PJ, Ohuchi FS. Hysteresis of the martensitic phase transition in magnetocaloric effect Ni-Mn-Sn alloys. Physical Review B. 2009; 79: 144407(1)–144407(9). DOI: 10.1103/PhysRevB.79.144407.

[21] Lakhani A, Dash S, Banerjee A, Chaddah P, Chen X, Ramanujan RV. Tuning the austenite and martensite phase fraction in ferromagnetic shape memory alloy ribbons of $Ni_{45}Co_5Mn_{38}Sn_{12}$. Applied Physics Letters. 2011; 99: 242503(1)–242503(3). DOI: 10.1063/1.3669510.

[22] Sarkar T, Roy S, Bhattacharya J, Bhattacharya D, Mitra CK, Dasgupta AKr. Thermal hysteresis of some important physical properties of nanoparticles. Journal of Colloid and Interface Science. 2008; 327: 224–232. DOI: 10.1016/j.jcis.2008.07.050.

[23] Kawamoto T, Abe S. Thermal hysteresis loop of the spin-state in nanoparticles of transition metal complexes: Monte Carlo simulations on an Ising-like model. Chemical Communications. 2005; No. 31, 3933–3935. DOI: 10.1039/b506643c.

[24] Atitoaie A, Tanasa R, Enachescu C. Size dependent thermal hysteresis in spin crossover nanoparticles reflected within a Monte-Carlo based Ising-like model. Journal of Magnetism and Magnetic Materials. 2012; 324: 1596–1600. DOI: 10.1016/j.jmmm.2011.12.011.

[25] Atitoaie A, Tanasa R, Stancu A, Enachescu C. Study of spin crossover nanoparticles thermal hysteresis using FORC diagrams on an Ising-like model. Journal of Magnetism and Magnetic Materials. 2014; 368: 12–18. DOI: 10.1016/j.jmmm.2014.04.054.

[26] Rego LGC, Figueiredo W. Magnetic properties of nanoparticles in the Bethe–Peierls approximation. Physical Review B. 2001; 64: 144424(1)–144424(7). DOI: 10.1103/PhysRevB.64.144424.

[27] Yalçın O, Erdem R, Demir Z. Magnetic properties and size effects of spin-1/2 and spin-1 models of core-surface nanoparticles in different type lattices. In: Abbass Hashim, editor. Smart Nanoparticles Technology: InTech; 2012. p. 541–560. DOI: 10.5772/34706.

[28] Yalçın O, Erdem R, Özüm S. Origin of the martensitic and austenitic phase transition in core-surface smart nanoparticles with size effects and hysteretic splitting. Journal of Applied Physics. 2014; 115: 054316(1)–054316(7). DOI: 10.1063/1.4864489.

[29] Özüm S, Yalçın O, Erdem R, Bayrakdar H, Eker HN. Martensitic and austenitic phase transformations in core-surface cubic nanoparticles. Journal of Magnetism and Magnetic Materials. 2015; 373: 217–221. DOI: 10.1016/j.jmmm.2014.03.044.

[30] Blume M, Emery VJ, Griffiths RB. Ising model for the λ transition and phase separation in He^3-He^4 mixtures. Physical Review A. 1971; 4: 1071–1077. DOI: 10.1103/PhysRevA.4.1071.

[31] Castán T, Vives E, Lindgård PA. Modeling premartensitic effects in Ni_2MnGa: A mean-field and Monte Carlo simulation study. Physical Review B. 1999; 60: 7071–7084. DOI: 10.1103/PhysRevB.60.7071.

[32] Berker AN, Wortis M. Blume–Emery–Griffiths–Potts model in two dimensions: phase diagram and critical properties from a position-space renormalization group. Physical Review B. 1976; 14: 4946–4963. DOI: 10.1103/PhysRevB.14.4946.

[33] Hoston W, Berker AN. Multicritical phase diagrams of the Blume–Emery–Griffiths model with repulsive biquadratic coupling. Physical Review Letters. 1991; 67: 1027–1030. DOI: 10.1103/PhysRevLett.67.1027.

[34] Kikuchi R. A theory of cooperative phenomena. Physical Review. 1951; 81. 988–1003.

[35] Meijer PHE, Keskin M, Bodegom E. A simple model for the dynamics towards metastable states. Journal of Statistical Physics. 1986; 45: 215–232. DOI: 10.1007/BF01033088.

[36] Erdinç A, Keskin M. Equilibrium and nonequilibrium behavior of the spin-1 Ising model in the quadrupolar phase. Physica A. 2002; 307: 453–468. DOI: 10.1016/S0378-4371(01)00620-3.

[37] Brück E, Trung NT, Ou ZQ, Buschow KHJ. Enhanced magnetocaloric effects and tunable thermal hysteresis in transition metal pnictides. Scripta Materialia. 2012; 67: 590–593. DOI: 10.1016/j.scriptamat.2012.04.037.

[38] Yanes R, Chubykalo-Fesenko O, Kachkachi H, Garanin DA, Evans R, Chantrell RW. Effective anisotropies and energy barriers of magnetic nanoparticles with Néel sur-

face anisotropy. Physical Review B. 2007; 76: 064416(1)–064416(13). DOI: 10.1103/PhysRevB.76.064416.

[39] Kita E, Oda T, Kayano T, Sato S, Minagawa M, Yanagihara H, Kishimoto M, Mitsumata C, Hashimoto S, Yamada K, Ohkohchi N. Ferromagnetic nanoparticles for magnetic hyperthermia and thermoablation therapy. Journal of Physics D: Applied Physics. 2010; 43: 474011(1)–474011(9). DOI: 10.1088/0022-3727/43/47/474011.

[40] Knittel A, Franchin M, Fischbacher T, Nasirpouri F, Bending SJ, Fangohr H. Micromagnetic studies of three-dimensional pyramidal shell structures. New Journal of Physics. 2010; 12: 113048(1)–113048(23). DOI: 10.1088/1367-2630/12/11/113048.

[41] Carrey J, Mehdaoui B, Respaud M. Simple models for dynamic hysteresis loop calculations of magnetic single-domain nanoparticles: application to magnetic hyperthermia optimization. Journal of Applied Physics. 2011; 109: 083921(1)–083921(17). DOI: 10.1063/1.3551582.

[42] Lee CF, Chang CL, Yang JC, Lai HY, Chen CH. Morphological determination of face-centered-cubic metallic nanoparticles by X-ray diffraction. Journal of Colloid and Interface Science. 2012; 369: 129–133. DOI: 10.1016/j.jcis.2011.12.053.

IntechOpen